Ocean Systems Engineering, *Vol. 15, No. 3 (2025) 241-270*
https://doi.org/10.12989/ose.2025.15.3.241

Bearing behavior assessment of wind turbines' shallow foundations, comparison of gravity-based foundations and suction buckets

Soheyl Hosseinzadeh* and Behrouz Gatmiri

School of Civil Engineering, College of Engineering, University of Tehran, Tehran, Iran

(Received April 22, 2025, Revised August 5, 2025, Accepted September 6, 2025)

Abstract. The rapid growth of offshore wind energy has driven the need for advanced foundation designs to support larger turbines in challenging marine environments. This study evaluates the performance of two key shallow foundation types for offshore wind turbines—gravity-based foundations (GBFs) and monopod suction buckets (MSBs)—using finite element analysis (FEA) in ABAQUS. Conducted at a site in the Dorood Oil Field in the Persian Gulf, the analysis compares soil stress, foundation settlement, lateral displacement, and rotation under gravitational and environmental loads. Eight GBF configurations with varying height-to-diameter ratios and ten MSB configurations with different skirt length to diameter ratios were examined. Results show that MSB foundations generally exhibit lower settlement and comparable lateral stability compared to GBFs, particularly for larger configurations, due to effective load transfer to deeper soil layers. However, GBFs demonstrate lower rotation angles at higher h/D ratios. Optimal configurations, GBF-1 and MSB-1, were identified as balanced designs offering reliable performance. These findings provide valuable insights for optimizing foundation design in offshore wind turbine projects, emphasizing the critical role of foundation geometry and soil-structure interaction.

Keywords: finite element analysis; gravity-based foundations; marine Geotechnics; monopod suction buckets; offshore foundations; offshore wind turbines

1. Introduction

Nowadays wind energy has the most use in the power generation industry. According to the EWEA reports 2.4% of total world power was provided by wind energy until 2000 whereas this rate has reached 15.6% during the last 20 years (EWEA 2016). To increase turbine output, the size of turbines is increasing. This issue requires larger and stronger supporting structures and foundations which presents a key challenge for civil engineers in offshore wind turbines (Wang *et al.* 2023).

Various foundation types used for fixed offshore wind turbines. Steel monopiles and concrete gravity foundations are the most commonly used foundations at sea due to their simple design principles, also applied onshore (Romero-Sánchez *et al*. 2024). The world's first offshore wind turbines, located at the Windy Bay wind farm in Denmark, used gravity foundations, making them

*Corresponding author, Dr., E-mail: s_hosseinzadeh@ut.ac.ir

http://www.techno-press.org/?journal=ose&subpage=7 ISSN: 2093-6702 (Print), 2093-677X (Online)

the oldest foundations in the industry (Potlock *et al*. 2023). According to EWEA (2016) and GWEC (2016) statistics, monopiles are the most widely used foundation type, while suction buckets are emerging as a new, practical, and cost-effective alternative, although they are still not mass-produced and are used in limited numbers for academic and laboratory experiments. Suction buckets were first used in the Fredericia wind farm in 2002 and the Horns Rev 2 wind farm in 2009, both located in the North Sea off Denmark (Mostafa *et al*. 2023a). Similar projects in the North Sea and Dogger Bank 2 have followed (Yetginer-Tjelta *et al*. 2022). Offshore turbine substructures are divided into fixed and floating types, with various designs offered based on seabed conditions and depths (Dagher *et al*. 2024). Fixed substructures transfer turbine loads directly to the seabed and are cost-effective for depths up to 100 meters (Tu *et al*. 2023).

Shallow foundations for wind turbines have attracted considerable attention due to their cost-effectiveness and adaptability to different soil conditions. Concrete gravity bases are among the most widely used shallow foundations for onshore wind turbines. These foundations are particularly beneficial in areas with suitable soil conditions, as they efficiently distribute the loads exerted by the turbine structure. For example, in Brazil, approximately 43.3% of wind turbines are supported by shallow foundations, mainly of the concrete gravity type, demonstrating their widespread application in specific geotechnical conditions (Nardelli and Futai 2022). The design of these foundations must account for significant bending moments and lateral forces caused by wind loads, as improper management of these forces can lead to structural instability (Flessati and Marveggio 2023). Recent studies highlight the importance of soil-structure interaction in the design of shallow foundations for wind turbines. The flexibility of tower supports and the dynamic response of the foundation system under varying load conditions are key factors influencing performance (Medeiros *et al*. 2024). The bearing capacity of shallow foundations is greatly influenced by soil type and moisture content. Research indicates that foundation performance varies significantly depending on these factors, making detailed geotechnical assessments necessary before installation (Joel and Oguanobi 2024). The interaction between the foundation and the underlying soil can cause differential settlement, which may weaken the turbine's structural integrity over time (Demirci 2023). Therefore, a thorough understanding of site-specific geotechnical properties is essential for optimizing foundation design. Beyond traditional concrete gravity foundations, innovative solutions are being developed to improve wind turbine performance. For instance, suction bucket foundations have shown enhanced bearing capacity and stability under dynamic loading conditions (Pan *et al*. 2022). Such advancements are crucial as the demand for renewable energy grows, driving the need for improved foundation technologies (Cui *et al*. 2024).

The finite element analysis (FEA) of wind turbine foundations has been an important area of research in geotechnical engineering during recent years. This method enables the simulation of complex interactions between soil, structure, and environmental forces, providing valuable insights into the stability and performance of these foundations under different conditions (Hosseinzadeh *et al*. 2024). For example McAuliffe (2024) used FEA to assess the fatigue and corrosion risks of offshore wind turbine support structures. The study emphasized the importance of accurately modeling stress concentration factors (SCFs) in gravity-based foundations for wind turbines. Also, Tu *et al*. (2022) analyzed the dynamic response of offshore wind turbines supported by gravity-based foundations (GBFs), using FEA. The study introduced a simplified time-domain method for predicting nonlinear dynamic responses, which is validated through comparisons with 3D finite element simulations (Tu *et al*. 2022). Moreover, Moraes (2024) presented a methodology for the structural analysis and design of gravity-based foundations for offshore wind turbines,

focusing on the challenges associated with the unique soil conditions in Northeast Brazil. The considered design criteria such as long-term damage, ultimate limit strength, and soil bearing capacity in accordance with international standards, providing a comprehensive framework for engineers involved in similar projects.

Additionally, many studies have focused on application of FEA in suction buckets behavior assessment. For instance, Bouneguet *et al.* (2023) presented a comprehensive analysis of the dynamic response of suction caisson foundations using a three-dimensional finite element model. The research examines soil–structure interaction under various loading conditions, emphasizing the influence of parameters such as caisson diameter and soil stiffness on dynamic behavior. Also, Suryasentana *et al.* (2022) explored the application of suction caisson foundations, in offshore wind turbine substructures. The study underscored the importance of accurately predicting foundation stiffness, which plays a critical role in the dynamic performance and fatigue life of the overall support structure. The authors introduced the OxCaisson model, an efficient tool for estimating foundation stiffness. Moreover, Mostafa (2023b) presented a comprehensive analysis of suction caisson foundations for offshore wind turbines using three-dimensional FEA. The study focused on the behavior of these foundations in clayey soils under lateral loading. On another hand, Wang *et al.* (2022) provided a comprehensive analysis of the bearing performance of suction bucket foundations for offshore wind turbines under both static and dynamic loads. The study compared monopile and suction bucket foundations within the geological conditions of the East China Sea, offering critical insights into their suitability for wind turbine substructures.

As previously mentioned, numerous studies have been conducted to investigate the behavior of shallow foundations for wind turbines. However, comparisons between the two most important types—gravity-based foundations (GBF) and monopod suction buckets (MSB)—have received less attention. Therefore, this study aims to evaluate the performance of these two shallow foundation concepts using FEA and examine the significance of factors such as higher weight and area in GBFs, as well as skirt length in MSBs. Additionally, the behavior of the sub-foundation soil beneath each of these foundation alternatives will be compared. The methodology is first presented, followed by the presentation and analysis of the results. Finally, the key findings and conclusions are summarized.

2. Methodology

2.1 General

This study utilizes FEA and numerical models to evaluate the performance of two key shallow foundation concepts for offshore wind turbine substructures. An overview of the methodology is provided in Fig. 1, with each step outlined as follows:

1- A suitable site for the offshore wind turbine is selected to evaluate the behavior of the sub-foundation soil, ensuring the results are based on real data.
2- Environmental and geotechnical data for the selected site are gathered, and an appropriate turbine is chosen for the area.
3- The foundation concepts, along with their geometric specifications, are defined, including GBFs of varying sizes and MSBs with different skirt lengths.
4- The loads imposed on the foundation, turbine structure, and hub are defined and calculated.

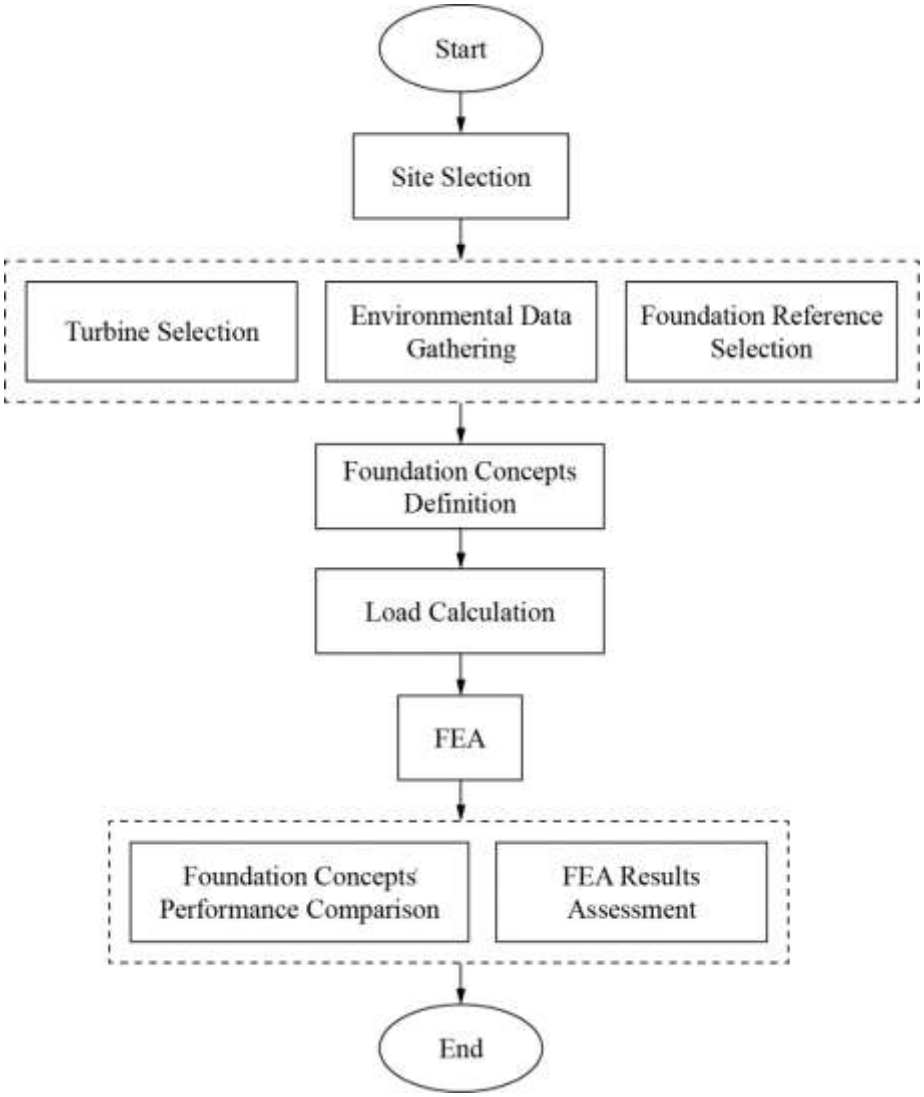

Fig. 1 Methodology Flowchart

5- A Finite Element Analysis is conducted using ABAQUS software to assess the behavior of the foundations and the soil beneath them.
6- The FEA results are presented and analyzed, allowing for a comparison of the behavior of different foundation concepts.
7- Finally, the results and conclusions are summarized and interpreted.

2.2 Site selection

Given the growing environmental challenges, including global warming, greenhouse gas emissions, and pollution from fossil fuels, the transition to clean energy has become increasingly

critical. Among clean energy sources, wind energy has been widely favored due to its availability and cost-free nature, with its use dating back to ancient windmills. Today, offshore wind energy, benefiting from high and steady wind speeds, is rapidly advancing. For instance, Europe, a leader in offshore wind energy, has expanded its capacity from 250 MW to 3300 MW in the past decades, while global offshore wind power generation has grown by 300% in the last five years (Song et al., 2024).

Initially, wind farms and oil platforms were built nearshore to simplify construction and reduce operational costs (Jacobsen *et al*. 2019). However, concerns about noise pollution, bird fatalities, and the adverse effects on coastal tourism and scenery prompted a shift toward offshore sites. As a result, modern wind farms are now located further from the coast, up to 120 kilometers offshore, and in deeper waters, moving from depths of 10 meters to 20–40 meters to access more favorable wind conditions (EWEA 2016).

Therefore, the suitable region for Locating wind turbine should be an area with a depth of 20 to 40 meters and a distance of more than 20 kilometers from the coast. To localize this study and enable gathering real data, suitable areas in the waters of the Persian Gulf, the Caspian Sea, and the Sea of Oman were examined. Ultimately, the Dorood Oil Field, located adjacent to Kharg Island in the northwestern Persian Gulf, was selected. This area not only has a depth close to 30 meters but also benefits from the availability of regional data due to extensive oil and gas production activities and the platforms constructed in the region.

2.3 Environmental data gathering

The selected region is characterized by specific environmental conditions critical for offshore design and operation. The mean sea level (MSL) is 31 meters, providing the baseline for depth measurements. For a 1-year return period, the region experiences a maximum wave height (H_{max}) of 6.5 meters with a corresponding peak wave period (T_{max}) of 8 seconds. The current velocity at the water surface level reaches 0.9 m/s, decreasing to 0.6 m/s near the seabed.

The wind load will be calculated using 1-minute gust (API 2019), the region is subject to 1-minute gust wind velocities of up to 25 m/s during a 1-year return period. In addition, the 3-hour wind speed average is 16 m/s which is considered as the turbine service wind.

2.4 Turbine specification

The primary criteria for selecting a wind turbine are the region's power generation potential and the generator's output capacity. Based on Eq. (1), turbine selection depends on wind speed, and rotor height. As the wind speed under normal operating conditions is approximately 16 m/s. To estimate this speed at a height of 90 meters, corresponding to the turbine tower height, the following equation is used

$$V_Z = V_{10}(\frac{z}{10})^{\alpha} \tag{1}$$

Where V_Z is the wind speed at height of Z, V_{10} is the wind speed at 10 meters, and α is a coefficient, typically $\frac{1}{7}$ under normal conditions (Sathe *et al*. 2011). Therefore, the wind speed at 90 meters height is approximately 22 m/s. For this study, the NREL 5 MW turbine has been selected as the reference turbine, as it performs optimally within a wind speed range of 11 to 25 m/s. The key specifications of this turbine are detailed in Table 1 (Jonkman *et al*. 2009).

Table 1 NREL 5 MW turbine specifications (Jonkman *et al*. 2009)

Property	Value
Rating	5 MW
Rotor Orientation, Configuration	Upwind, 3 Blades
Control	Variable Speed, Collective Pitch
Drivetrain	High Speed, Multiple-Stage Gearbox
Rotor,1 Hub Diameter	126 m, 3 m
Hub Height	90 m
Cut-In, Rated, Cut-Out Wind Speed	3 m/s, 11.4 m/s, 25 m/s
Cut-In, Rated Rotor Speed	6.9 rpm, 12.1 rpm2
Rated Tip Speed	80 m/s
Overhang, Shaft Tilt, Precone	5 m, 5°, 2.5°
Rotor Mass	110,000 kg
Nacelle Mass	240,000 kg
Tower Mass	347,460 kg
Coordinate Location of Overall CM	(-0.2 m, 0.0 m, 64.0 m)

2.5 Foundation reference selection

The working principle of a gravity-based foundation is to resist sliding and overturning through its self-weight. Herein the MSB foundation geometric modeling of the gravity foundation is inspired by the Thornton Bank in Belgium. This foundation consists of a concrete chamber that is filled with sand and gravel after being placed in its final position (Kerckhof *et al*. 2010).

On another hand the working principle of suction bucket foundations combines the mechanisms of piles and gravity foundations. In suction bucket foundations, due to their installation process and the creation of relative vacuum pressure between the foundation and the soil, any applied impact causes the suction to restore the foundation to its original position. In this type of foundation, the weight of the soil inside the bucket, along with the friction between the soil and the bucket walls, contributes to the stability of the structure. In this paper the geometric design of this foundation is inspired by the Dogger Bank wind farm located in the North Sea, belonging to the United Kingdom (Yetginer-Tjelta *et al.* 2022).

2.6 Numerical modeling

To evaluate the behavior of candidate shallow foundations, a three-dimensional Finite Element Model (FEM) was created in ABAQUS 6.14 (Hosseinzadeh *et al*. 2025). The assumptions and features of the numerical model are detailed in this section.

2.6.1 Foundation model

GBF: The foundation model consists of a 45-meter wire element with a solid circular cross-section for the transitional part. This is rigidly connected to a solid element below, which includes the concrete foundation and its fill materials. The rigid section is 17 meters high, and the diameter of the upper part, where the foundation rests, is designed to match the Thornton Bank

dimensions, measuring 6.5 meters. The fill materials at the base of the foundation are heavier, while the upper sections are filled with lighter materials. The concrete used in this foundation is C45-grade concrete. Skirts were not used in this foundation since the aim was to compare the gravity-based system with the suction bucket system. The gravity foundation was designed to also represent skirtless foundations. In the analyzed model, the GBF is placed at a depth of 3.5 meters below the seabed. To define the soil-structure interaction, the foundation was assumed to be embedded in the soil. A sample of gravity-based foundation model has been depicted in Fig. 2(a).

The aim of this research is not foundation design and just the behavior of foundation is to be assessed. Therefore, to investigate the effect of varying diameters for gravity foundations, eight gravity foundation concepts were evaluated with h/d ratios of 0.75, 1, 1.25, 1.5, 1.75, 2, 2.5, and 3 named as GBF-0.75, GBF-1, GBF-1.25, GBF-0.5, GBF-1.75, GBF-2, GBF-2.5, and GBF-3 respectively, similar to the ratios of turbine foundations at the Thornton Bank wind farm in Belgium Fig. 2(a). The height of the conical section (h) is set at 17 meters, and the height of the transitional section (h_t) is 45 meters. The base diameter of the foundation was calculated by multiplying the height of the conical section (h) by the specified ratios (h/D).

MSB: a monopod suction bucket consists of an inverted steel bucket with the transitional section placed on top of it. At the connection between these two parts, ten triangular steel stiffeners have been incorporated into the bucket section to provide the required stiffness for absorbing the transferred moment and preventing the steel plate from tearing. The software model follows the same design. Also, a wire element with a steel pipe cross-section and a diameter of 6.5 meters represents the transitional section. This section is rigidly connected to the stiffened part, which is modeled using shell elements. The lateral stiffness of the component is enhanced by ten triangular shell elements. The turbine tower is placed on the foundation at a height similar to the gravity foundation. To achieve this, the transitional section was modeled with a height of 60 meters, 30 meters of which is submerged in water while the remaining 30 meters is above the water surface. Fig. 2(b) provides a schematic view of the modeled monopod suction bucket foundation.

The part of the suction bucket embedded in the soil is referred to as the skirt. The skirt plays a critical role in the tensile load-bearing capacity of this type of foundation. This capacity is provided through the friction between the skirt wall and the soil, the cohesion of the soil itself, and the weight of the soil trapped inside the inverted bucket. These factors depend on the skirt depth. For modeling soil-structure interaction, the skirt was assumed to be embedded in the soil, and negative pressure forces were simulated by attaching the soil surface to the foundation surface.

To evaluate the effect of increasing skirt length on shallow foundations, ten suction bucket concepts were evaluated with skirt-to-diameter (h/D) ratios of 0.1, 0.2, 0.25, 0.3, 0.4, 0.5, 0.75, 1, 1.25, and 1.5 named as MSB-0.1, MSB-0.2, MSB-0.25, MSB-0.3, MSB-0.4, MSB-0.5, MSB-0.75, MSB-1, MSB-1.25, and MSB-1.5 respectively. For all these foundations, the diameter was kept constant at 23.5 meters, matching the diameter of the turbine foundations at the Thornton Bank wind farm. The only difference among the designs is the skirt length.

2.6.2 Soil model

Geotechnical data are among the most critical parameters for foundation performance. According to gathered information, the soil in the targeted region consists of 12 layers up to a depth of approximately 100 meters, predominantly clay layers with some interspersed sandy layers. Detailed soil information for the region is presented in Table 2.

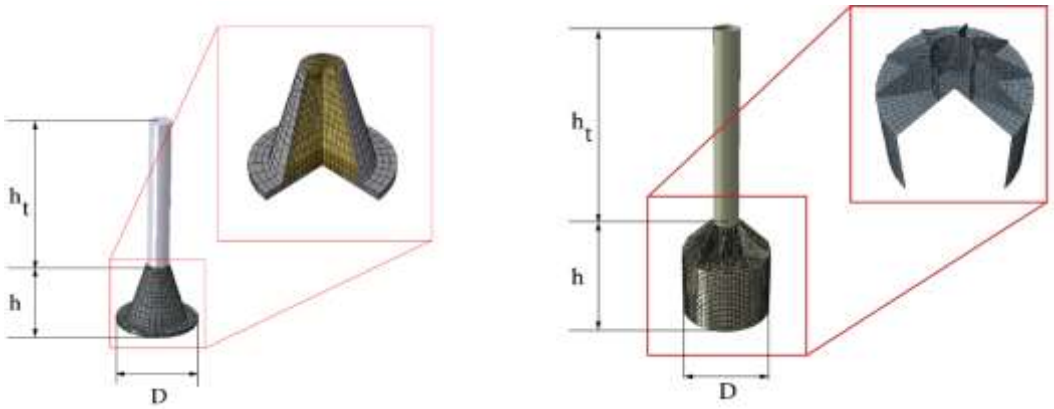

(a) (b)

Fig. 2 Foundation model sample

Table 2 Doroud Region Soil Properties

Layer Name	Soil Type	Depth (m)	Unit Weight (kN/m³)	Shear Strength (kPa)
1a	Clay	0–5	5	2–8
1b	Clay	5–7.15	6	8–8
2	Sand	7.15–10.55	8.3	-
3	Clay	10.55–13	8.5	50–50
4	Clay	13–31.2	8.7	40–65
5	Clay	31.2–50.1	8.7	65–80
6	Sand	50.1–53.1	10.6	-
7	Clay	53.1–56.95	9.5	85–95
8	Sand	56.95–58.5	10	-
9	Clay	58.5–62	9	110–140
10a	Clay	62–95	9.5	140–200
10b	Clay	95–100.82	10	200–200

As illustrated in Fig. 3 the soil element is modeled cylindrical. The total depth of the soil is 100.82 meters, starting with soft clay at the surface and transitioning to very stiff clay at the base. The diameter of the soil cylinder is set to 400 meters. At its center, a 200-meter diameter cylinder is modeled using deformable 3D solid elements (C3D8). The outer part is modeled using infinite 3D elements (Cin3D8) to simulate an unbounded seabed connected to the infinite ocean floor. The infinite elements are elastic by nature and require a high length-to-width ratio. Therefore, the infinite region includes a single long mesh along the diameter, and no direct loads are applied to this section.

Considering the 23.5-meter diameter foundation plate at the Thornton Bank wind farm and the 200-meter soil cylinder, the soil diameter is 8.5 times the foundation diameter. This ratio is sufficient for obtaining accurate results in finite element analysis, as a ratio greater than 5 is

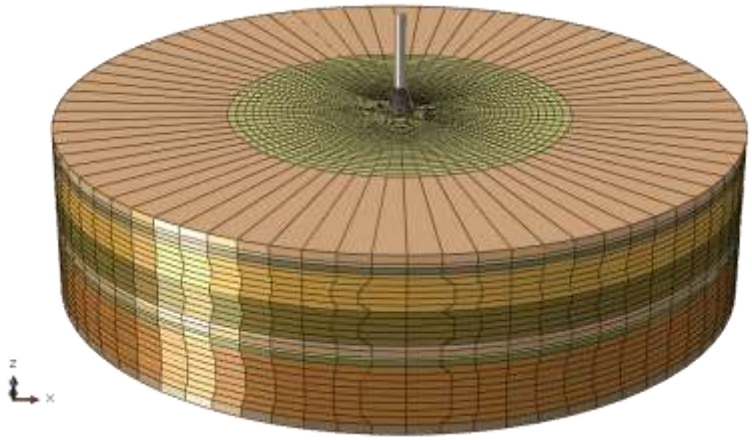

Fig. 3 Soil Model Scheme

recommended. The soil's plasticity is defined using the Mohr-Coulomb failure criterion. To account for the lateral pressure of the soil layers not explicitly modeled, predefined lateral forces were applied to the modeled soil. These forces represent the lateral pressure exerted by the surrounding seabed. The lateral earth pressure coefficients were calculated using Eq. (2), considering yielding values of 0.74 for clay particles and 0.42 for sand particles.

$$k = 1 - sin\phi \tag{2}$$

2.6.3 Loads

According to the DNV offshore turbine design code (DNV 2019), the loads acting on offshore wind turbines are categorized into five groups: permanent, operational variable, environmental, accidental, and displacement loads. This study focuses on permanent design loads related to operational conditions, as opposed to temporary design loads relevant to construction phases.

Permanent loads include constant factors such as the mass of structural components (rotor, hub, nacelle, tower, substructure, foundation, etc.), permanent equipment, and internal/external hydrostatic pressures under stable conditions. Operational variable loads arise during normal operations, including crane loads, docking of vessels, temporary equipment, and pressures from consumable fluids or gases. Environmental loads are variable during operation and include wind, hydrodynamic forces (drag and inertia from waves), earthquakes, tidal effects, and snow/ice loads. Accidental loads result from unexpected events like dropped objects, explosions, impacts, fires, or collisions (e.g., with helicopters or ships). Displacement loads stem from deformation or movement of components, such as thermal expansion, dimensional changes during fabrication, or foundation settlement. The loads implemented on the structure are explained in this section.

2.6.4 Rotor trust calculations

The wind load that is blowing with a speed of v and effect in an area of A is as follows (Gasch and Twele 2012)

$$P_{Wind} = \frac{1}{2}\rho A v^3 \tag{3}$$

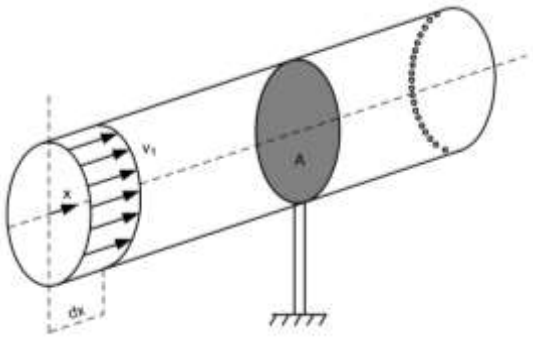

Fig. 4 Schematic of steam flow in a pipe with an area of A (Gasch and Twele 2012)

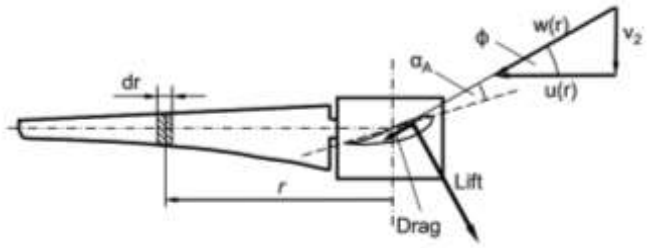

Fig. 5 The aerodynamic forces on the blade ring element (Gasch and Twele 2012)

Where ρ is air density. Wind power is kinematic energy of the wind that passes a special area in a special time by air mass (Fig. 4) (Gasch and Twele 2012)

$$E = \frac{1}{2}mv^2 \tag{4}$$

$$\dot{m} = A\rho\frac{dx}{dt} = \rho Av \tag{5}$$

Lift and drag forces in the blades of wind turbines are created that their magnitudes in the blade element of length dr at the radius r

$$dL = \frac{\rho}{2}cw^2C_L(\alpha_A)dr \tag{6}$$

$$dD = \frac{\rho}{2}cw^2C_D(\alpha_A)dr \tag{7}$$

Where c is the Chord length and $\alpha_A$is considered as the blade angle along with the wind direction. drag force and lift force are created in the direction of relative speed and perpendicular to it respectively. These two forces are dividable into two forces in tangent direction with rotating circular plate of blades and wind direction that they are called circumferential force and thrust force respectively and considering Fig. 5 they are as follows (Gasch and Twele 2012)

$$dU = \frac{\rho}{2}cw^2dr(C_D cos\phi - C_L sin\phi) \tag{8}$$

$$dT = \frac{\rho}{2} cw^2 dr(C_D sin\phi + C_L cos\phi) \tag{9}$$

The common point of all presented equations for calculation force, power, and torques related to wind turbines is their dependency on relative speed angle (γ). The calculation of all parameters for different γ to design turbines is repetitive and overwhelming work and therefore some diagrams were presented for simplifying the calculations so that different features of turbines for different γ are calculated, but in dimensionless turbines, the reference variable for these diagrams is tip speed ratio or λ that all features of turbine are stated according to it and upstream wind speed ($v1$) is also used as reference speed ($\lambda = \frac{\Omega R}{v_1}$). In the way that all parameters are divided into a dynamic force for

$$F_{dyn} = \frac{\rho}{2} \pi R^2 v_1^2 \tag{10}$$

and a constant according to λ. Actually, the dynamic force is the multiplication of dynamic force ($\frac{\rho}{2} v^2$) and the circle area of turbine blades (πR^2) so we have [5]

$$\begin{cases} T = F_{dyn} C_T(\lambda) = \frac{\rho}{2} \pi R^2 v_1^2 C_T(\lambda) \\ M = R F_{dyn} C_M(\lambda) = \frac{\rho}{2} \pi R^3 v_1^2 C_M(\lambda) \\ P = v_1 F_{dyn} C_P(\lambda) = \frac{\rho}{2} \pi R^2 v_1^3 C_P(\lambda) \end{cases} \tag{11}$$

Three constants of C_T, C_M, and C_P were given in Eq. (11) which are thrust, moment, and power factors. These factors are influenced by tip speed, and various diagrams are provided for different speed ratios. The pitch control adjusts the γ angle, leading to changes in other parameters while maintaining constant dynamic pressure. As a result, the power, thrust, and moment factors are affected. Based on the turbine's maximum power and the pitch angle required to prevent generator damage, the critical parameters related to thrust load are evaluated. For a tip speed ratio of 2.33, the corresponding blade pitch angle is 30 degrees. At this setting, the power coefficient (C_P) is 0.13, while the thrust coefficient (C_T) is 0.18 (Gasch and Twele 2012).

2.6.5 Turbine tower and transition piece wind load calculation

The implied wind load on the tower and transition piece as a slender element is calculated by Eq. (12) (API 2019).

$$F_W = \frac{\rho}{2} v_1^2 C_S A \tag{12}$$

Where C_S is shape coefficient, and A is the area of object.

As the wind turbine itself is not modeled in the ABAQUS software; instead, its effects are incorporated into the foundation model. Therefore, the wind load affected on the rotor and tower will be imposed to the foundation structure as an equal load and moment. The actual model is shown in Fig. 6(a), while the equivalent foundation model created in ABAQUS is presented in Fig. 6(b).

2.6.6 Wave load

The wave implies force on the underwater part of foundation and wind implies the force on the part of the foundation that is upper than water level. Drag force is defined by the wave and wind

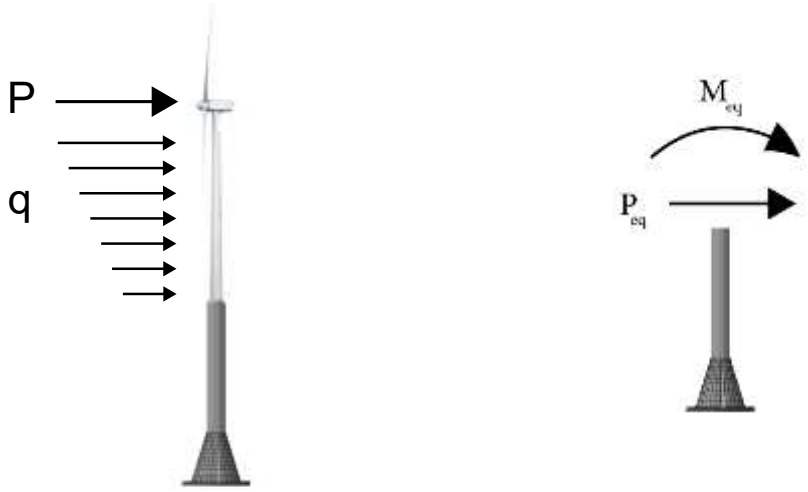

Fig. 6 Load implementation scheme

speed profile and it is implied on the structure. Fluid drag force on the turbine is calculated by Eq. (13) (API 2019)

$$F_D = A\frac{\rho}{2}C_D D\Delta V_{fn}\left|\Delta V_{fn}\right| \tag{13}$$

Where C_D is Drag coefficient and D is object effective diameter. Fluid inertia force causes that structure has more inertia resistance than acceleration and also the added mass is calculated in that, Inertia force on the structure is calculated as Eq. (14)

$$F_I = \mathrm{A}\rho_\omega \frac{\pi D^2}{4}[C_M A_{fn} - C_A A_{pn}] \tag{14}$$

Where A is load defined amplitude. The buoyancy force has two components including hydrostatic pressure that is resulted from water weight to the average level of the sea and dynamic pressure that it is the factor of those wave creations. When buoyancy force and wave are applied simultaneously, they are added to hydrostatic forces considering the change of water level.

2.6.7 Gravity and hydrostatic load

A weight load is applied to the entire model, with the gravitational acceleration considered as 9.81 m/s^2. Also, the weight of the turbine components implemented manually on the foundation. Moreover, the hydrostatic load imposed to foundation structure assuming water density equal to $1025\frac{kg}{m^3}$.

2.6.8 Model verification

Validation is a critical step in ensuring the reliability of numerical modeling results, particularly when simulating complex models (Hosseinzadeh *et al.* 2025). To evaluate the validity of the model, a model similar to an experimental test performed by Wang *et al*. (2017) was developed and its

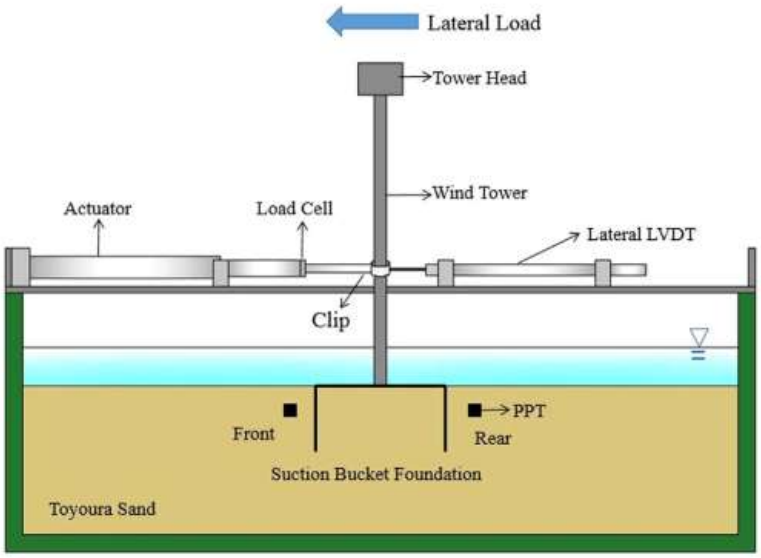

Fig. 7 Elevation view of test package (Wang *et al*. 2017)

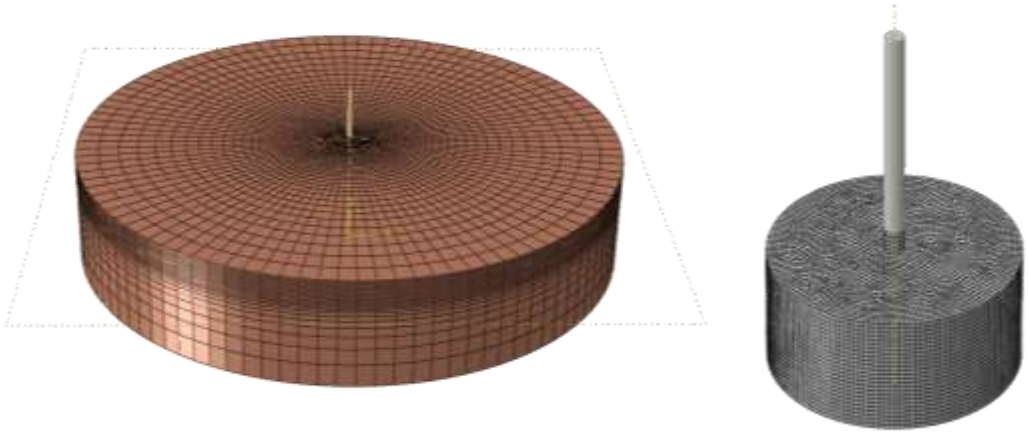

Fig. 8 Validation model scheme

results were compared with their findings. The study utilized centrifuge modeling, an advanced experimental technique conducted on the 20 g-ton geotechnical centrifuge at Case Western Reserve University, with models subjected to a 50 g acceleration to replicate prototype-scale conditions. The tests were load-controlled, applying static lateral loads via an electrical actuator, with a load cell recording load and a Lateral Variable Displacement Transducer (LVDT) measuring displacement (Fig. 7). A steel suction bucket foundation model with aspect ratio of 0.5 was used along with a simplified wind turbine model and Toyoura sand was prepared. Model was installed at 1 g, and lateral load was applied at 50 g.

Table 3 Reference model specifications

Category	Property	Value
Bucket Foundation (Wang *et al*. 2017)	Material	Steel
	Young's Modulus (E)	200 GPa
	Poisson's Ratio (μ)	0.30
	Friction Coefficient (Foundation-Soil)	0.5
	Diameter	5 m
	Skirt Length	2.5 m
	Thickness	0.0125 m
Soil (Toyoura Sand) (Yang *et al*. 2017)	Type	Sand
	Dry Unit Weight	14 kN/m³
	Relative Density	~30%
	Internal Friction Angle (ϕ)	25°
	Dilation Angle	5°
	FE Model	Mohr-Coulomb
	Young's Modulus (E_s)	10 MPa
	Poisson's Ratio (μ)	0.30
	Diameter	50 m
	Depth	10 m

Table 4 Comparison of Centrifuge Test and Numerical Analysis Results

Lateral Load (kN)	d_h *by* Wang *et al.* (2017)	d_h *in validation model*	Deviation
131.3	0.15 m	0.207 m	27.5%
142.6	0.30 m	0.402 m	25.3%
170.3	0.45 m	0.548 m	21.4%

Therefore, a finite element model was developed in ABAQUS based on the reference model's specifications and incorporating the modeling methodology established in the present study. The reference includes 12 models, among which the one with loose-saturated sand and an h/D ratio of 0.5 was selected for validation. The model consists of two components—soil and bucket—as shown in Fig. 8, and follows the specifications listed in Table 3.

The modeling was carried out in two static steps: the first step applied the gravity load, and the second applied a lateral load. The static load, consistent with the centrifuge tests, was implemented as a linear monotonic load in a force-controlled manner. The primary objective of these static tests was to evaluate the static lateral bearing capacity. During the static test, the load was increased continuously and linearly over time. In accordance with the methodology of the present study, the ultimate lateral capacity was not assessed. Instead, the lateral load–displacement response under static loading was analyzed at three load levels—131.3, 142.6, and 170.3—corresponding to normalized deflections of 3%, 6%, and 9%, respectively. Here, normalized deflection is defined as the lateral deflection (d_h) divided by the bucket diameter (D). Accordingly, the lateral deflection of the model was calculated and compared with the centrifuge test results, as presented in Table 4.

Table 5 Mesh size sensitivity analysis results

d_e/D	0.2	0.1	0.08	0.04	0.02
d_h	0.148 m	0.203 m	0.207 m	0.207 m	0.207 m

The results indicate that the FE model produces reliable predictions, demonstrating satisfactory agreement with the centrifuge test data. The observed discrepancies are attributed to simplifications in the constitutive model and potential variations in soil properties that were not fully captured in the numerical simulation.

To ensure the robustness of the FE model, a mesh sensitivity analysis was performed for the case with a lateral load of 131.3 kN. The mesh structure in the foundation region was designed using structured C3D8R elements, with cubic elements of equal dimensions near the foundation. A sweep meshing technique was employed, whereby the mesh size increased progressively with distance from the foundation to optimize computational efficiency. Five different mesh sizes were evaluated, with element dimensions (d_e) normalized by the foundation diameter (D) as follows: $d_e/D = 0.2, 0.1, 0.08, 0.04, and\ 0.02$. The results of the mesh sensitivity analysis are presented in Table 5.

Based on the analysis, a mesh size of d_e/D = 0.08 was selected, as it provided the most accurate results while maintaining computational efficiency. Finer mesh sizes (d_e/D = 0.04 and 0.02) yielded identical deflections, indicating convergence, but were deemed unnecessarily computationally intensive.

Given the higher complexity of the MSB model and the similarity in soil modeling approaches between the MSB and the GBF concepts, it is inferred that the GBF model can achieve comparable performance to the MSB model when the same methodology is applied.

3. Results and discussion

3.1 Soil stress comparison

The model has been analyzed in two general static steps. The first step examines the effects of gravity and hydrostatic pressure before applying lateral loads. The second step evaluates the foundation and soil behavior after the application of environmental loads. Fig. 9 shows the soil stress contours from the first step, and below it, the sub-foundation soil behavior after the application of lateral loads is illustrated.

As can be observed in Fig. 9, in gravity-based foundations, the stress is imposed just beneath the foundation, whereas in suction bucket foundations, the maximum stress is transferred to deeper soil layers. Additionally, inside the suction bucket foundation, the stress is shown to be higher compared to the outside. Furthermore, when foundation is subjected to lateral loading and rotation, a stress concentration is observed in gravity-based foundations, whereas in suction bucket foundations, this does not occur, and the load distribution is demonstrated to be more balanced. To provide a more comprehensive comparison between the two foundation types, this section is focusing on comparing the stress values across different geometries of both foundations under varying loading conditions.

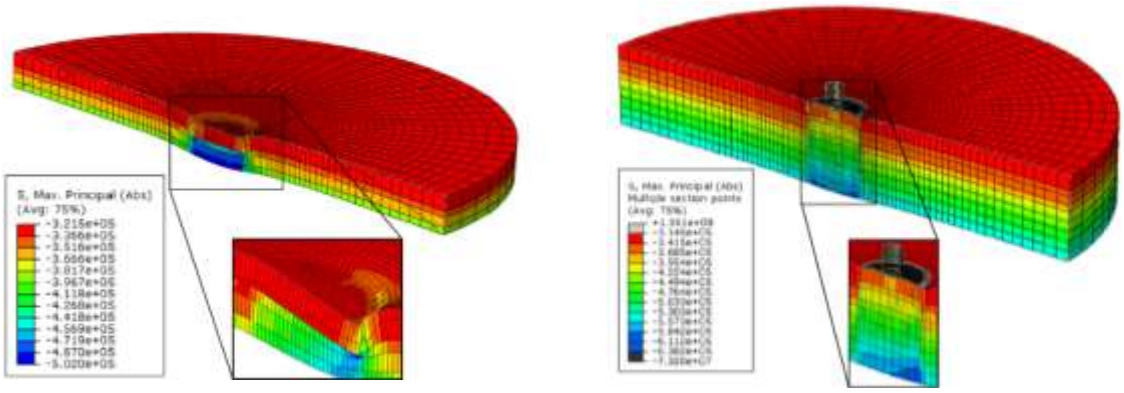

(a) (b)

Fig. 9 FEM model soil stress contour in gravity-based foundation model (a) and monopod suction bucket (b)

Fig. 10 depicts the soil Maximum Von-Mises Stress (MVMS) in the sub-foundation soil under gravitational and hydrostatic loads during Step 1 while the gravity and hydrostatic loads are imposed. MVMS is a scalar measure of stress used to predict stress in materials under complex loading. It represents the maximum equivalent uniaxial stress within the structure (Hosseinzadeh and Bahaari 2025).

For GBF foundations, the stress is reported to be highest at -4.66e+05 Pa for GBF-0.75, reflecting a significant concentration of load due to the limited contact area relative to the foundation's self-weight. A reduction is observed to -4.53e+05 Pa at GBF-1, attributed to an optimized load distribution facilitated by an increased contact area. However, an unexpected increase is noted to -4.63e+05 Pa at GBF-1.25 and -4.70e+05 Pa at GBF-1.5, which is considered to arise from an imbalance between the foundation's weight and contact area, potentially exacerbated by geometric changes such as the conical transition section. A gradual decrease is subsequently recorded from -4.69e+05 Pa at GBF-1.75 to -4.60e+05 Pa at GBF-3, indicating that the effect of enhanced contact area becomes dominant beyond an h/D ratio of 1.75. These non-monotonic fluctuations are interpreted as a result of the complex soil-structure interaction.

For MSB foundations, the stress is found to increase consistently from -4.12e+05 Pa at MSB-0.1 to -6.28e+05 Pa at MSB-1.5, a trend explained by the progressive deepening of the skirt to a depth of 35 m. This increase should not be interpreted as a deterioration in foundation performance with increasing skirt length; rather, it is attributed to the penetration of the foundation base into deeper, more resistant, and denser soil layers. The load resulting from the weight of the overlying soil layers is seen to be added to the stress induced by the foundation load in the soil beneath the base, enhanced by the confinement effect and frictional resistance between the skirt walls and the soil. The steady increase is considered to reflect the gradual mechanical response of the soil profile to the deepening skirt, where the load is effectively transferred and resisted through the combined effects of overlying soil weight and shear strength in deeper layers.

The stress distribution after applying lateral environmental loads is shown in Fig. 11. The results indicate that GBF foundations apply less stress as their size increases. The maximum soil stress beneath the foundation decreases from 660 kPa in GBF-0.75 to 460 kPa in GBF-3, highlighting the greater influence of foundation area compared to its weight when environmental loads are applied.

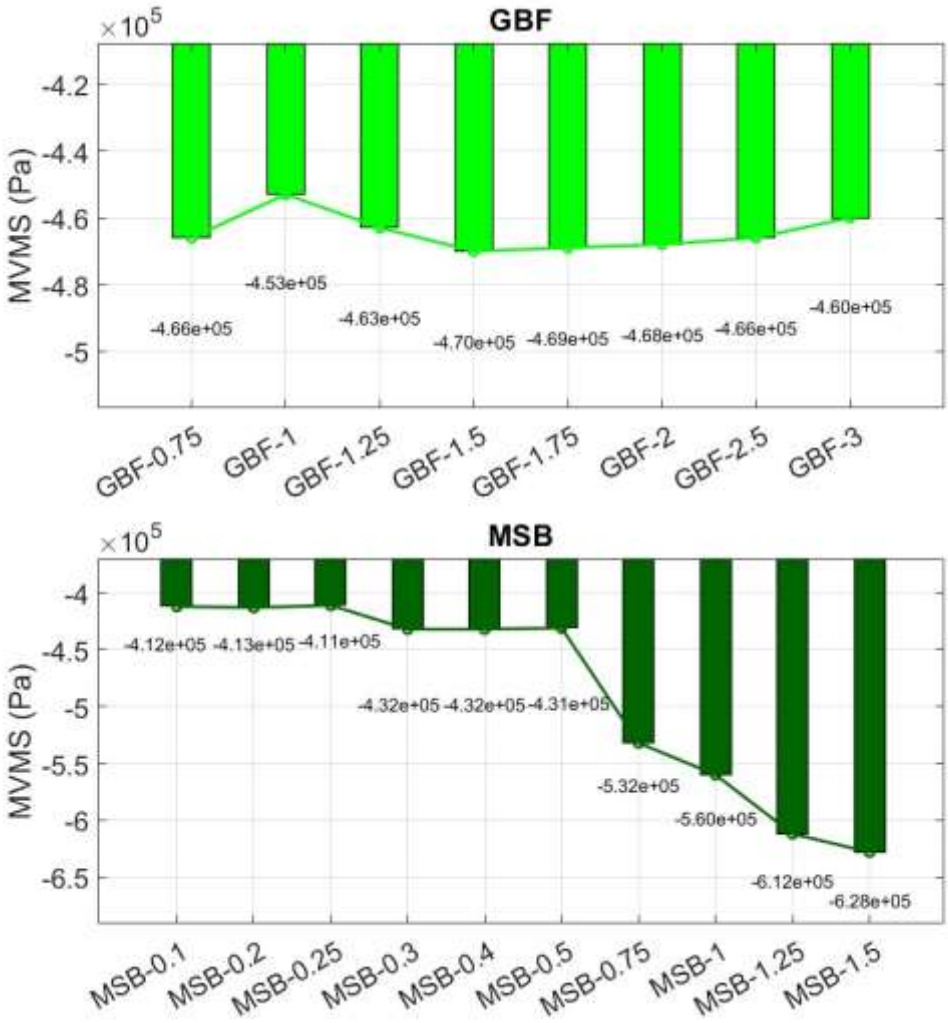

Fig. 10 Maximum soil stress under the foundation load during step 1

On the other hand, the maximum soil stress under the foundation load during step 2, revealing a non-monotonic trend for MSB foundations. The stress has been observed to increase from MSB-0.1 to MSB-0.2, followed by a decrease and stabilization up to MSB-0.5, and a subsequent rise toward MSB-1.5, which has been attributed to the competing effects of skirt length, upper layers' soil weight, and soil layer properties. The initial stress increase has been linked to the concentration of load in deeper layers with shorter skirts, while the reduction and stability up to MSB-0.5 have been associated with improved load distribution due to skirt friction in comparison with soil weight. The stress increase from MSB-0.75 to MSB-1.5 has been influenced by the growing weight of upper soil layers and potential changes in soil stiffness and density with depth, overwhelming the effect of skirt length.

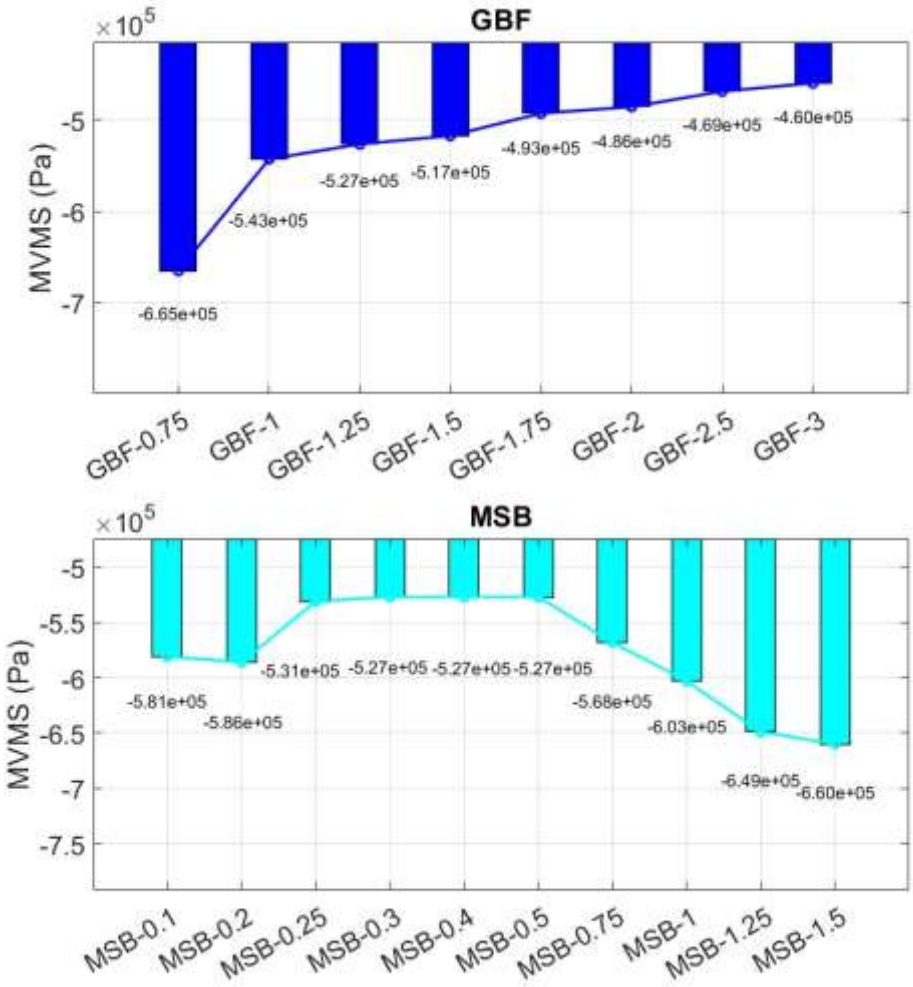

Fig. 11 Maximum soil stress under the foundation load during step 2

As indicated before, due to the influence of the structure's weight and the soil weight, the results shown in Figs. 10 and 11 are not appropriate for an accurate comparison of the foundations performance. To examine the effect of environmental loads independently from soil self-weight and gravitational loads, the stress in Step 1 was subtracted from that in Step 2, as shown in Fig. 12.

The results indicate that GBF foundations impose less stress as the foundation area increases, ranging from 200 kPa to approximately 0 in the studied foundations. Similarly, the results for MSB foundations show that a longer skirt reduces the soil stress beneath it. The stress level remains constant from MSB-0.25 to MSB-0.5 and decreases significantly further in foundations deeper than MSB-0.75. It worth noting that soil stress beneath MSB has been increased slightly from MSB-0.1 to MSB-0.2 and from MSB-0.75 to MSB-1.0, contrary to the expected reduction with increased skirt length. This minor rise has been technically justified by the transitional load

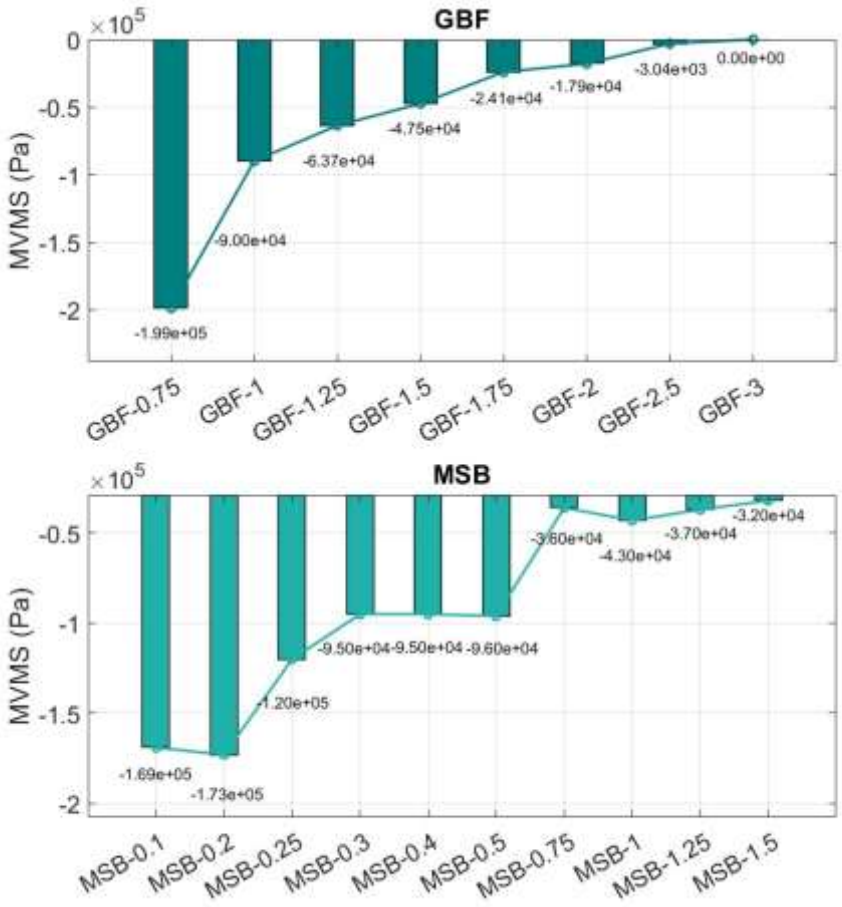

Fig. 12 Pure lateral load effects on soil stress

transfer in shorter skirts, where the confinement effect has not fully matured, leading to a localized stress concentration beneath the foundation base. Additionally, the slight increase from MSB-0.75 to MSB-1.0 has been attributed to the enhanced moment effect induced by longer skirts, which directs a modest portion of the environmental load toward the foundation base, consistent with the embedded interaction model.

3.1 Foundation settlement comparison

Soil settlement beneath the foundation is a critical parameter in the design and construction of a foundation. The analysis results indicate that the self-weight of the structure primarily contributes to soil settlement, and during the application of lateral loads, no significant change in settlement, is observed. A contour plot for vertical displacement for each of GBF and MSB foundations are shown in Fig. 13. To provide better insight into the foundation settlement behavior, the deformation scale factor was adjusted to 1:50.

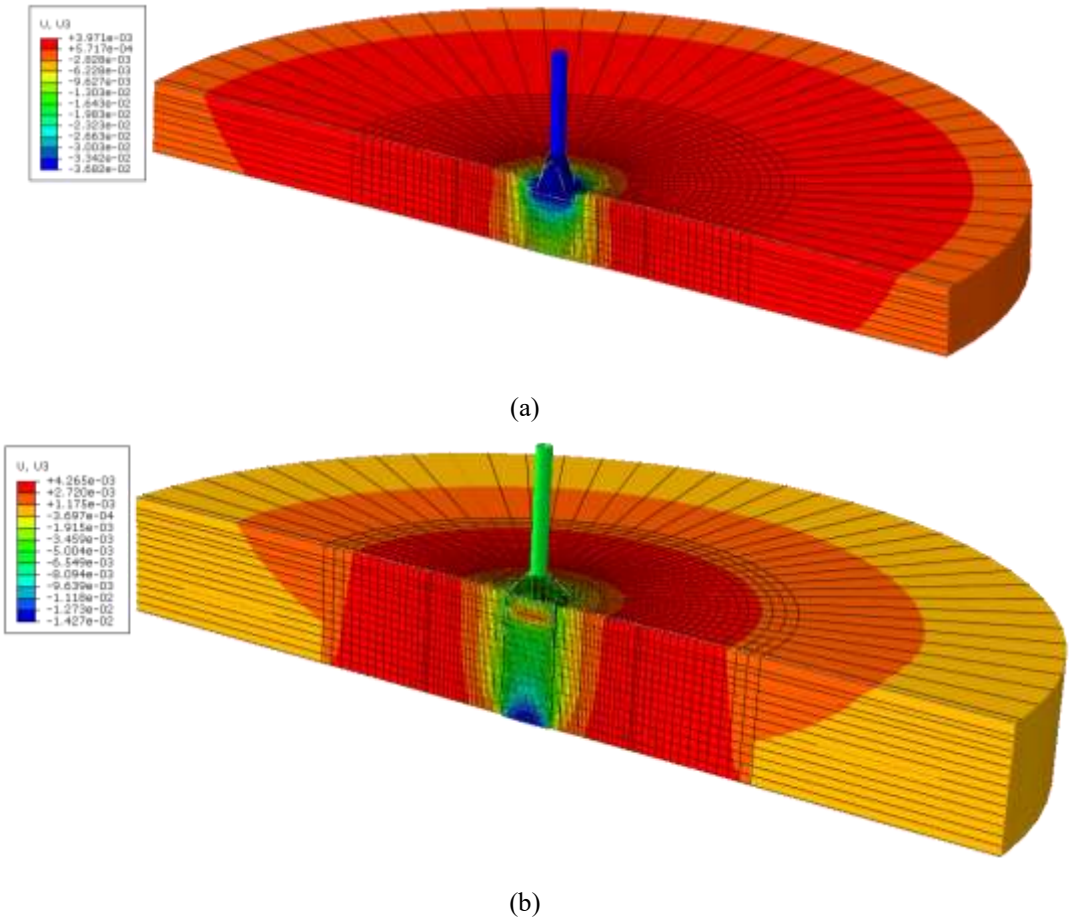

(a)

(b)

Fig. 13 FEM model Vertical deflection contour in gravity-based foundation model (a) and monopod suction bucket (b)

Fig. 13(a) illustrates the contours of vertical displacements for a sample gravity-based foundation (GBF). Both the foundation and the underlying soil are found to have settled uniformly by approximately 3.5 centimeters, which is attributed to the substantial weight of the concrete foundation under gravitational loading .A gradual reduction in settlement has been observed with increasing distance from the foundation, consistent with the geometric distribution of the gravitational load as described by principles such as Boussinesq's theory (Terzaghi *et al*. 1996). The surrounding soil has been noted to heave by about 3 millimeters, a phenomenon linked to lateral displacement caused by the significant settlement beneath the foundation and the soil's flexibility. In the same way, as is observed in Fig. 13(b), the soil inside the bucket has been found to experience greater settlement (approx. 5 mm) compared to the surrounding soil (approx. 2 mm), which is attributed to the confinement effect induced by the skirts. A portion of the soil near the top of the bucket has been observed to swell upward, likely due to lateral stress relief and material displacement resulting from the gravitational loading. The greatest settlement (approx. 14 mm) has been recorded directly beneath the center of the foundation, outside the bucket, which is explained

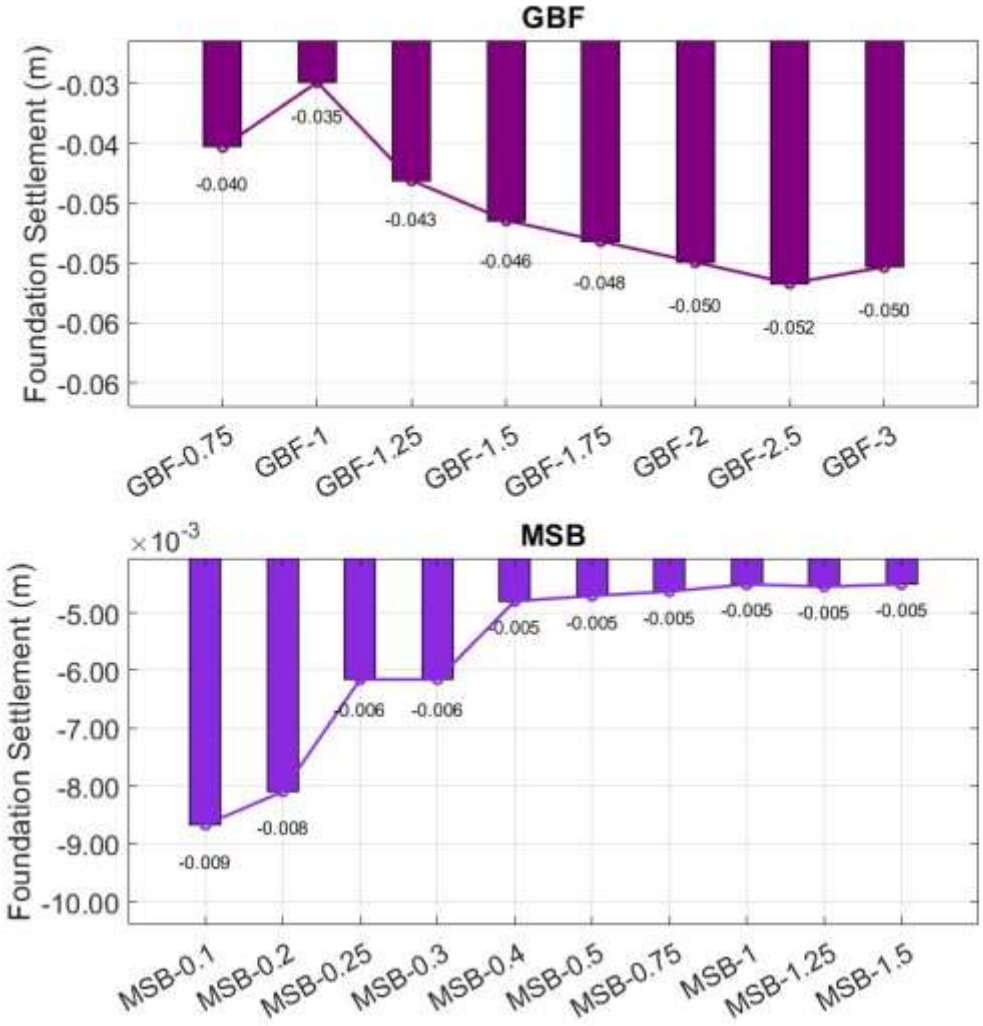

Fig. 14 Maximum foundations' Settlement in different foundation concepts

by the concentrated gravitational load in an area lacking lateral support from the skirt. Additionally, the soil slightly beyond the foundation perimeter has been noted to heave by 4 mm, a phenomenon linked to the lateral displacement caused by the significant settlement beneath the center.

The results shown in Fig. 14 were obtained through the analysis of the maximum settlement observed during Step 1. The analysis of the vertical settlement diagram for GBF and MSB has been conducted, revealing distinct behavioral patterns. In GBF, the settlement has been observed to decrease from GBF-0.75 (0.040 m) to GBF-1 (0.035 m) due to an optimized h/D ratio, followed by an increase to GBF-2.5 (0.052 m) attributed to the dominant effect of additional foundation weight, and a subsequent reduction beyond GBF-2.5 (0.050 m) linked to enhanced load distribution over a larger contact area. In MSB, a significant reduction in settlement has been noted

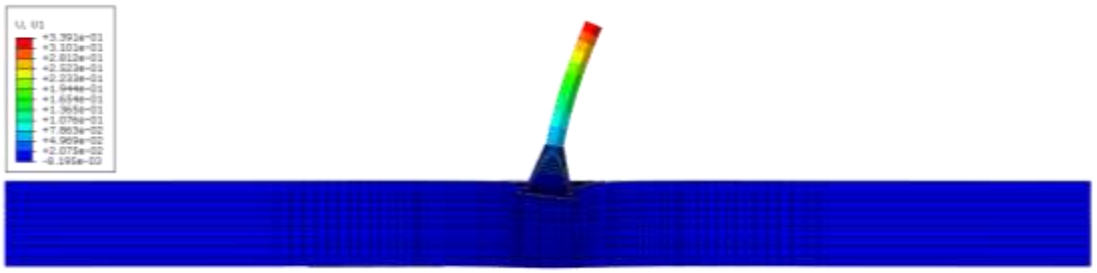

(a)

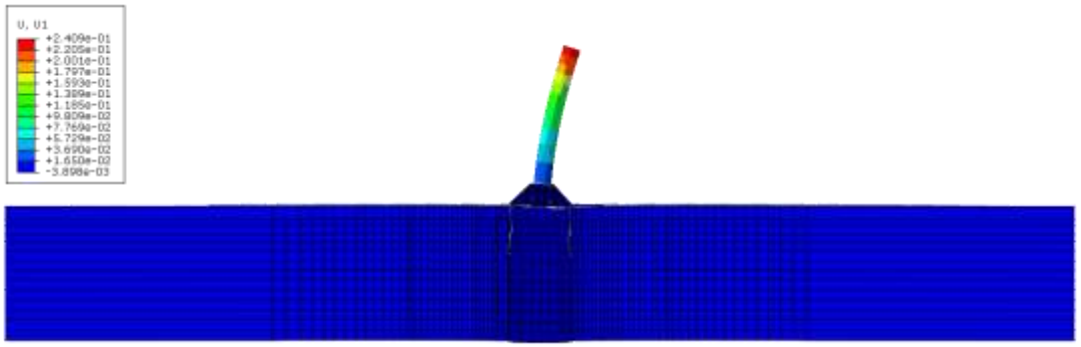

(b)

Fig. 15 FEM model lateral deflection contour in gravity-based foundation model (a) and monopod suction bucket (b)

from MSB-0.2 (0.009 m) to MSB-0.25 (0.006 m) owing to improved skirt confinement, followed by a notable increase from MSB-0.3 to MSB-0.4 (0.005 m) due to altered stress distribution, with settlement stabilizing at higher ratios (0.005 m) as the load is effectively transferred to deeper soil layers.

The results confirm that the minimum settlement of GBF foundations occurs in GBF-1, measuring 4 cm, and it increases as the foundation size grows. In contrast, the settlement of MSB foundations decreases as the skirt length increases. The findings indicate that for larger foundations, the GBF concept can lead to greater settlement due to its higher weight, whereas MSB foundations are a better choice as they do not impose additional load on the soil due to self-weight.

3.2 Turbine deflections comparison

One of the critical parameters for foundation design is lateral displacement, which significantly affects the stability and performance of the structure. In Fig. 15, a sample of the lateral displacement results has been presented with a 1:50 scale. As observed, the maximum displacement has been identified at the uppermost element, which is found to be consistent with the foundation's rotation and influenced by the differing structural configurations at the transitional section (concrete in the gravity-based foundation and steel in the suction bucket

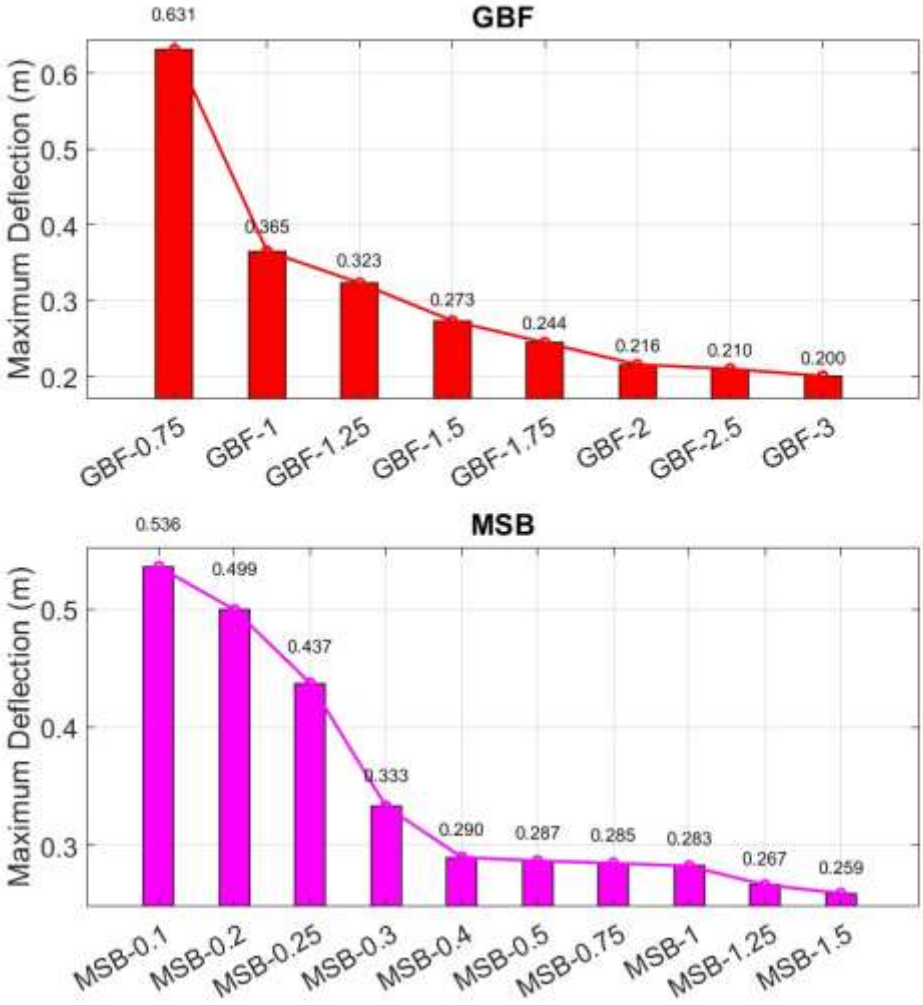

Fig. 16 Maximum Foundations' deflection in different concepts

foundation), ultimately leading to the calculated maximum lateral displacement values for the foundation. Additionally, the results have demonstrated that lateral loadings were unable to displace the foundation itself, with displacement being observed solely at the transitional section.

Fig. 16 presents the maximum lateral displacements for different foundation concepts. As shown in the figure, the lateral displacement at the tower-to-substructure connection (top of the substructure) shows that the lightweight GBF-0.75 foundation exhibits approximately 60 cm of horizontal displacement at this level. Medium-weight foundations (GBF-1, 1.25, 1.5) show around 30 cm of displacement, while heavy foundations (GBF-1.75, 2, 2.5, 3) experience about 20 cm.

According to the MSB foundation results, the foundation with the shortest skirt, MSB-0.1, exhibits the highest lateral deformation, while the foundation with the longest skirt, MSB-1.5,

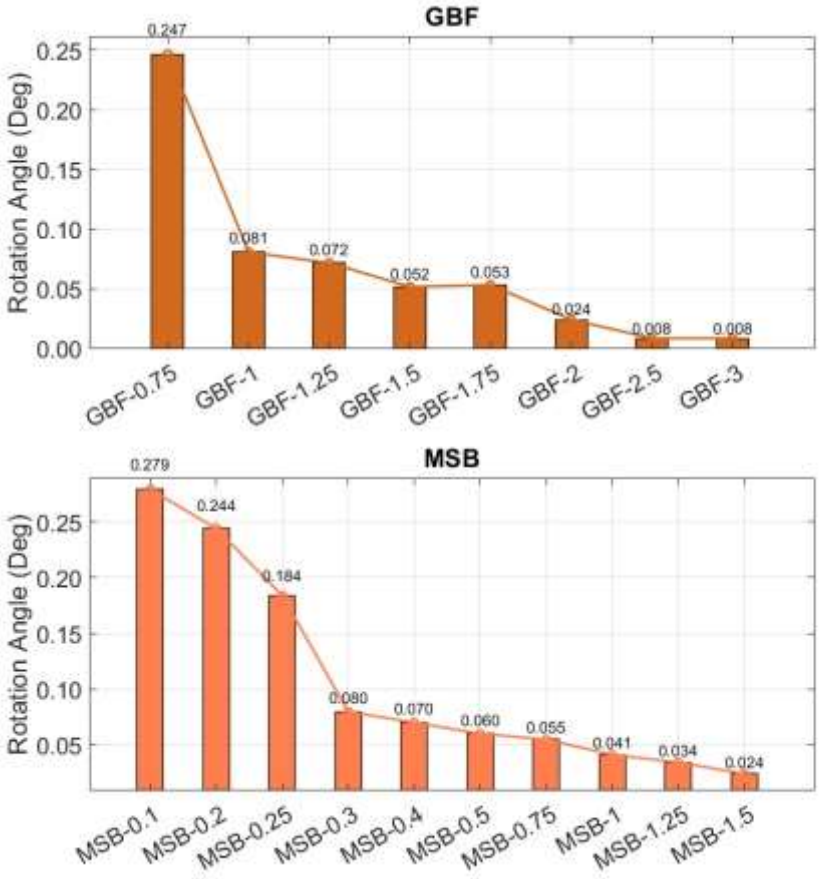

Fig. 17 Foundations' rotation angle

experiences the least displacement. The highest lateral displacement at the tower-to-foundation connection occurs in MSB-0.1, reaching 54 cm. it can be also inferred, this displacement decreases with increasing skirt length and stabilizes at around 30 cm for foundations MSB-0.4 and deeper ones.

Overall, the comparison of different foundation concepts indicates that both increased foundation mass in GBFs and greater embedment depth in MSBs contribute effectively to minimizing lateral displacements. While both foundation types exhibit comparable levels of horizontal deformation, MSB foundations show a marginally superior performance in lateral stability.

3.3 Maximum footing rotation

Due to the nature of lateral loads, moment generation, and asymmetric settlement, the foundation experiences rotation which is considered an undesirable phenomenon. The rotation of

the foundations can be perceived by Fig. 15. Fig. 17 is presented to illustrate the maximum rotation angles for studied concepts of GBF and MSB foundations. For GBF foundations, the rotation angle is reported as 0.247 degrees for GBF-0.75, which is subsequently reduced to 0.008 degrees for GBF-3. This decrease is attributed to the enhanced load distribution and reduced overturning moment resulting from the increased contact area and self-weight of the foundation. In contrast, MSB foundations are shown to exhibit a rotation angle of 0.279 degrees for MSB-0.1, which is decreased to 0.024 degrees for MSB-1.5. This reduction, observed to accelerate after an h/D ratio of approximately 0.5, is linked to the critical role played by the skirt in transferring loads to deeper soil layers and improving stability.

A comparison between the two foundation types is conducted, revealing that both demonstrate improved performance with increasing h/D ratios. However, GBF foundations are noted to achieve lower rotation angles at the highest ratios compared to MSB foundations. This advantage is attributed to the significant self-weight and increased toe length of the footing of GBF foundations, which are found to enhance stability against overturning moments at larger sizes. In contrast, the skirt mechanism of MSB foundations is observed to provide effective load transfer to deeper soil layers, resulting in reduced rotation angles up to an h/D ratio of approximately 1.5, though further increases yield diminishing returns. Nevertheless, for GBF foundations, the rotation angle is seen to stabilize at 0.008 degrees after GBF-2.5, suggesting a limitation in the effectiveness of additional size increases beyond this point.

3.4 Foundation types evaluation

Eight gravity-based foundation concepts and ten monopod suction bucket concepts were modeled under gravitational and environmental loads, and the soil behavior beneath the foundations was assessed to evaluate the performance of the two most popular shallow foundation types for wind turbines.

Based on the comprehensive evaluation of stress, displacement, settlement, and rotation, three representative cases have been selected for each foundation type and labeled accordingly:

- **Worst case**: the configuration with the poorest overall performance.
- **Best case**: the configuration demonstrating the most favorable performance across all criteria.
- **Optimal case**: a balanced configuration that is neither overly conservative nor underperforming.

The corresponding results for these representative cases are presented in Table 6, providing a comparative overview of each foundation's behavior under lateral loading conditions. Accordingly, GBF-1 and MSB-1 have been identified as the optimal alternatives for comparison. These cases represent well-balanced designs that offer reliable performance without excessive conservative assumptions.

Regarding settlement, GBF foundations experience settlements between 3 and 4 cm, whereas in all MSB concepts, settlement remains below 1 cm. In terms of foundation rotation angle, GBFs rotate between 0.008 and 0.25 degrees, while MSBs exhibit rotation in the range of 0.02 to 0.28 degrees.

According to the results, GBF foundations perform better in smaller sizes. However, in larger foundations, their higher weight can be detrimental, making MSB concepts a far better choice for wind turbine substructures.

Table 6 Results summary

Foundation Type	GBF			MSB		
Case	Worst case	Best case	Optimal case	Worst case	Best case	Optimal case
Soil Stress (kPa) "Under pure lateral load effect"	GBF-0.75 200	GBF-3 0	GBF-1 90	MSB-0.1 170	MSB-1.5 32	MSB-1 40
Horizontal Displacement (cm)	GBF-0.75 63	GBF-3 20	GBF-1 36	MSB-0.1 50	MSB-1.5 26	MSB-1 28
Foundation settlement (cm)	GBF-0.75 4	GBF-1 3	GBF-1 3	MSB-0.1 1	MSB-1.5 0.5	MSB-1 0.5
Foundation rotation angle (Deg)	GBF-0.75 0.25	GBF-3 0.008	GBF-1 0.08	MSB-0.1 0.28	MSB-1.5 0.02	MSB-1 0.04

4. Conclusions

This study provides a detailed comparison of gravity-based foundations (GBFs) and monopod suction bucket (MSB) foundations for offshore wind turbines, employing finite element analysis (FEA) to evaluate their performance under gravitational and environmental loads at a site in the Dorood Oil Field, Persian Gulf. The analysis focused on critical parameters, including soil stress, foundation settlement, lateral displacement, and rotation, across eight GBF configurations with varying height-to-diameter (h/D) ratios and ten MSB configurations with different skirt lengths. The results reveal distinct performance characteristics for each foundation type, offering valuable insights for optimizing offshore wind turbine foundation design.

MSB foundations demonstrated superior performance in terms of settlement, consistently achieving values below 1 cm across all configurations, compared to 3–4 cm for GBFs. This advantage is attributed to the skirt mechanism, which effectively transfers loads to deeper, more resistant soil layers, enhancing stability and reducing soil deformation. The increased skirt length in MSB designs further improves load distribution, particularly in deeper soil layers with higher shear strength, as evidenced by the progressive reduction in settlement from MSB-0.2 (0.009 m) to MSB-1.5 (0.005 m). Additionally, MSB foundations exhibited comparable lateral stability to GBFs, with lateral displacements stabilizing at around 30 cm for skirt lengths beyond MSB-0.4, highlighting their robustness under environmental loads.

In contrast, GBF foundations showed advantages in minimizing rotation angles, particularly at higher h/D ratios. The rotation angle decreased significantly from 0.247 degrees for GBF-0.75 to 0.008 degrees for GBF-3, driven by the increased self-weight and larger contact area, which enhance resistance to overturning moments. However, this comes at the cost of higher settlement due to the substantial weight of GBFs, which can exacerbate soil deformation, especially in larger configurations. The non-monotonic stress behavior in GBFs, with stress peaking at GBF-1.5 (-4.70e+05 Pa) before decreasing, underscores the complex interplay between foundation geometry and soil-structure interaction.

Optimal configurations, GBF-1 and MSB-1, were identified as balanced designs that provide reliable performance without excessive conservatism. GBF-1 achieves a settlement of 3 cm, a rotation angle of 0.08 degrees, and a lateral displacement of 36 cm, while MSB-1 records a

settlement of 0.5 cm, a rotation angle of 0.04 degrees, and a lateral displacement of 28 cm. These configurations strike a balance between performance and practicality, avoiding the excessive weight of larger GBFs or the deeper embedment of MSBs, which may increase construction complexity.

The findings highlight the critical influence of site-specific geotechnical conditions on foundation performance. The layered soil profile at the Dorood Oil Field, characterized by clay and interspersed sand layers, significantly affects stress distribution and settlement behavior. MSB foundations are particularly advantageous in such conditions due to their ability to leverage deeper soil layers, whereas GBFs are better suited for scenarios where minimizing rotation is a priority. These results underscore the importance of foundation design for specific soil properties and environmental conditions to ensure long-term stability and cost-effectiveness.

References

API. (2019), Planning, Designing, and Constructing Fixed Offshore Platforms - Load and Resistance Factor Design. *RP 2A-LRFD*.

Bouneguet, S., Messioud, S. and Dias, D. (2023), "Vertical and horizontal dynamic response of suction caisson foundations", *Studia Geotechnica Et Mechanica*, **45**(1), 1-13. https://doi.org/10.2478/SGEM-2022-0018.

Cui, L., Amani, S., Gabr, M., Kumari, W.G.P., Ahmed, A., Ozcan, H., Horri, B.A. and Bhattacharya, S. (2024), "Synergistic hybrid marine renewable energy harvest system", *Energies*, **17**(5). https://doi.org/10.3390/EN17051240.

Dagher, J.H., Goupee, A.J. and Viselli, A.M. (2024), "Optimized floating offshore wind turbine substructure design trends for 10–30 MW turbines in low-, medium-, and high-severity wave environments", *Designs*, **8**(4). https://doi.org/10.3390/DESIGNS8040072.

Demirci, H.E. (2023), "Geotechnical preliminary design of onshore wind turbine foundations", *Erzincan Üniversitesi Fen Bilimleri Enstitüsü Dergisi*, **16**(3), 756-781. https://doi.org/10.18185/ERZIFBED.1306867.

DNV. (2019), Design of offshore wind turbine structure. *DNV-OS-J101*. https://pdfcoffee.com/dnv-os-j101-design-of-offshore-wind-turbine-structurepdf-pdf-free.html.

EWEA. (2016). *The European offshore wind industry-key trends and statistics 2015*.

Flessati, L. and Marveggio, P. (2023), "A simplified method for calculating the accumulation of irreversible ro-tations of wind turbine shallow foundations", *Symposium on Energy Geotechnics 2023*, 1-2. https://doi.org/10.59490/SEG.2023.608.

Gasch, R. and Twele, J. (2012), Wind power plants: Fundamentals, design, construction and operation, second edition. *Wind Power Plants: Fundamentals, Design, Construction and Operation*, 2nd Ed., 1-548. https://doi.org/10.1007/978-3-642-22938-1/COVER.

GWEC. (2016), *Global Wind Report*. Wind Energy Technology.

Hosseinzadeh, S., Bahaari, M., Abyani, M. and Taheri, M. (2025), "Data-driven remaining useful life estimation of subsea pipelines under effect of interacting corrosion defects", *Appl. Ocean Res*., https://doi.org/https://doi.org/10.1016/j.apor.2025.104438.

Hosseinzadeh, S. and Bahaari, M.R. (2025), "A novel approach for reliability assessment of corroded offshore pipelines using machine learning and random sampling", *Ocean Eng.,* **341**, 122523. https://doi.org/10.1016/j.oceaneng.2025.122523.

Hosseinzadeh, S., Bahaari, M.R. and Abyani, M. (2024), "Reliability Assessment for pipelines corroded by longitudinally aligned defects", *Ocean Eng.*, https://doi.org/https://doi.org/10.1016/j.oceaneng.2024.118625

Hosseinzadeh, S., Bahaari, M.R. and Abyani, M. (2025), "Machine learning models development to predict

corroded pipeline behavior considering defects interaction", *Int. J. Mar. Technol.*, PrePrint.
Jacobsen, H.K., Hevia-Koch, P. and Wolter, C. (2019), "Nearshore and offshore wind development: Costs and competitive advantage exemplified by nearshore wind in Denmark", *Energy for Sustainable Development*, **50**, 91-100. https://doi.org/10.1016/J.ESD.2019.03.006.
Joel, O.T. and Oguanobi, V.U. (2024), "Geotechnical assessments for renewable energy infrastructure: Ensuring stability in wind and solar projects", *Eng. Sci. Technol. J.*, **5**(5), 1588-1605. https://doi.org/10.51594/ESTJ.V5I5.1110.
Jonkman, J., Butterfield, S., Musial, W. and Scott, G. (2009), *Definition of a 5-MW Reference Wind Turbine for Offshore System Development*. http://www.osti.gov/bridge.
Kerckhof, F., Rumes, B., Jacques, T., Degraer, S. and Norro, A. (2010), "Early development of the subtidal marine biofouling on a concrete offshore windmill foundation on the Thornton Bank (southern North Sea): first monitoring results", *Underwater Technol.*, **29**(3), 137-149. https://doi.org/10.3723/UT.29.137.
McAuliffe, J., Baisthakur, S., Broderick, B. and Fitzgerald, B. (2024), "Corrosion fatigue analysis of NREL's 15-MW offshore wind turbine with time-varying stress concentration factors", *J. Phys. : Conference Series*, **2767**(6). https://doi.org/10.1088/1742-6596/2767/6/062023.
Medeiros, I.D.S., Bello, M.I.M. da C.V. and de Lima, D.M. (2024), "Influence of soil-structure interaction on the behavior of the tower-foundation system of a horizontal-axis wind turbine", *Struct. Des. Tall Spec.*, **33**(16). https://doi.org/10.1002/TAL.2163.
Moraes, P.M.H. de, Ellwanger, G.B. and Nascimento, L.S.do. (2024), "Structural analysis integration methodology for gravity-based foundation design of offshore wind turbines in Brazil", *J. Eng. Res*., **4**(26), 1-9. https://doi.org/10.22533/AT.ED.3174262401111.
Mostafa, O., Arab, M.G. and Omar, M. (2023a), "3D finite element modeling of suction caissons used as foundations for offshore wind turbines in clayey soils", *Adv. Sci. Technol.*, **129**, 51-59. https://doi.org/10.4028/P-PXXXU9.
Mostafa, O., Arab, M.G. and Omar, M. (2023b), "3D finite element modeling of suction caissons used as foundations for offshore wind turbines in clayey soils", *Adv. Sci. Technol.*, **129**, 51-59. https://doi.org/10.4028/P-PXXXU9.
Nardelli, A. and Futai, M.M. (2022), "Assessment of Brazilian onshore wind turbines foundations", *Revista IBRACON De Estruturas E Materiais*, **15**(5). https://doi.org/10.1590/S1983-41952022000500008.
Pan, X., He, B., Yuan, Z., Xu, S., Xu, D., Jiang, Z., Shi, L. and Sun, H. (2022), "Effect of reinforced bucket on bearing capacity and natural frequency of offshore wind turbines using pile–bucket foundation", *Adv. Civil Eng.*, **2022**(1). https://doi.org/10.1155/2022/9569102.
Potlock, K.M., Temple, A.J. and Berggren, P. (2023), "Offshore construction using gravity-base foundations indicates no long-term impacts on dolphins and harbour porpoise", *Mar. Biol.*, **170**(8). https://doi.org/10.1007/S00227-023-04240-1.
Romero-Sánchez, C., Padrón, L.A., Álamo, G.M., Medina, C., Aznárez, J.J. and Maeso, O. (2024), "Comparative study of the influence of kinematic interaction on the seismic response of monopile and jacket supported offshore wind turbines", *J. Phys. : Conference Series*, **2647**(11). https://doi.org/10.1088/1742-6596/2647/11/112002.
Sathe, A., Gryning, S.E. and Peña, A. (2011), "Comparison of the atmospheric stability and wind profiles at two wind farm sites over a long marine fetch in the North Sea", *Wind Energy*, **14**(6), 767-780. https://doi.org/10.1002/WE.456.
Song, D., Shen, G., Huang, C., Huang, Q., Yang, J., Dong, M., Joo, Y.H. and Duić, N. (2024), "Review on the application of artificial intelligence methods in the control and design of offshore wind power systems", *J. Mar. Scie. Eng*., **12**(3), 424. https://doi.org/10.3390/jmse12030424.
Suryasentana, S.K., Burd, H.J., Byrne, B.W. and Shonberg, A. (2022), "A Winkler model for suction caisson foundations in homogeneous and non-homogeneous linear elastic soil", *Géotechnique*, **72**(5), 407-423. https://doi.org/10.1680/JGEOT.19.P.172.
Terzaghi, K., Peck, R.B. and Mesri, G. (1996), *Soil mechanics in engineering practice*. 549.
Tu, W., He, Y., Liu, L., Liu, Z., Zhang, X. and Ke, W. (2022), "Time domain nonlinear dynamic response analysis of offshore wind turbines on gravity base foundation under wind and wave loads", *J. Mar. Sci.*

Eng., **10**(11). https://doi.org/10.3390/JMSE10111628.
Tu, Z., Zhang, C., Liu, H. and Zhu, R. (2023), "Hydrodynamic analysis of a multi-pile-supported offshore wind turbine integrated with an aquaculture cage", *J. Mar. Sci. Eng.*, **11***(*9). https://doi.org/10.3390/JMSE11091830
Wang, B., Qin, T., Yuan, C., Li, L., Yuan, M. and Li, Y. (2022). "Analysis of bearing performance of monopile and single suction bucket foundation for offshore wind power under horizontal load", *Geofluids*, https://doi.org/10.1155/2022/4163240.
Wang, W., Gao, Y., Qiu, D., Wang, Z., Nie, P. and Ma, H. (2023), "Research on the strengthening and retrofitting methods of existing wind turbine foundations with embedded-ring", *IET Renew. Power Generation.*, **17**(16), 3793-3803. https://doi.org/10.1049/RPG2.12882.
Wang, X., Yang, X. and Zeng, X. (2017), "Centrifuge modeling of lateral bearing behavior of offshore wind turbine with suction bucket foundation in sand", *Ocean Eng.*, **139**, 140-151. https://doi.org/10.1016/J.OCEANENG.2017.04.046.
Yang, X., Wang, X. and Zeng, X. (2017), *Numerical simulation of the lateral Loading capacity of a bucket foundation*, Geotechnical Frontiers 2017, 112-121.
Yetginer-Tjelta, T.I., De Sordi, J., Caferri, L., Rose, M., Duffy, C., Lunne, T., Blaker, Ø., Strandvik, S. and Meyer, V. (2022), "The role of cone penetration testing in the dogger bank offshore wind farm", *Cone Penetration Testing 2022 - Proceedings of the 5th International Symposium on Cone Penetration Testing, CPT* 1156-1163.

MK

Abbreviation

API	American Petroleum Institute
C3D8	3D Solid Element
C3D8R	3D Solid Reduced Integration Element
Cin3D8	3D Infinite Element
C_D	Drag Coefficient
C_L	Lift Coefficient
C_M	Moment Coefficient
C_P	Power Coefficient
C_S	Shape Coefficient
C_T	Thrust Coefficient
DNV	Det Norske Veritas
EWEA	European Wind Energy Association
FEA	Finite Element Analysis
FEM	Finite Element Model
GBF	Gravity-Based Foundation
GWEC	Global Wind Energy Council
H_{max}	Maximum Wave Height
LVDT	Linear Variable Displacement Transducer
MSB	Monopod Suction Bucket
MSL	Mean Sea Level
MVMS	Maximum Von-Mises Stress
NREL	National Renewable Energy Laboratory
SCF	Stress Concentration Factor
T_{max}	Peak Wave Period